Multicontinuum homogenization and its relation to nonlocal multicontinuum theories

Yalchin Efendiev [a], Wing Tat Leung [b],*

[a] *Department of Mathematics, Texas A&M University, College Station, TX 77843, USA*
[b] *Department of Mathematics, City University of Hong Kong, Hong Kong*

A B S T R A C T

In this paper, we present a general derivation of multicontinuum equations and discuss cell problems. We present constraint cell problem formulations in a representative volume element and oversampling techniques that allow reducing boundary effects. We discuss different choices of constraints for cell problems. We present numerical results that show how oversampling reduces boundary effects. Finally, we discuss the relation of the proposed methods to our previously developed methods, Nonlocal Multicontinuum Approaches.

1. Introduction

One of the commonly used approaches for multiscale problems includes homogenization and its variations [6,21,23,24,30, 7,15], where effective properties at each macroscale grid or point are computed. These computations are often based on local solutions computed in a representative volume element (or coarse grid) centered at a macroscale point. Homogenization-based approaches assume scale separation and that the local media can be replaced by a homogeneous material. As a result, it is assumed that the solution average in each coarse block approximates the heterogeneous solution within that coarse block.

In many cases, even within the scale separation realm, homogenization (as discussed above) is not sufficient and the coarse-grid formulation requires multiple homogenized coefficients. These approaches are developed for different applications [27,4,28,1,19,8,3,5,9,2] and we call them (following the literature) multicontinuum approaches. Multicontinuum approaches assume that the solution average is not sufficient to represent the heterogeneous solution within each coarse block. In the derivation of multicontinuum approaches, there are typically several assumptions: (1) continua definitions; (2) physical laws describing the interaction among continua; and (3) conservation laws deriving final equations. Various assumptions are typically made in deriving these models. The first such approach is presented in [27], where the author assumes existence of continua that have different equilibrium temperatures among each other (continua) and formulates empirical laws for interaction among continua. In more rigorous approaches related to porous media [4,28,3,26], the continua are assumed to be fracture and matrix regions. In our earlier works [14,13,31], we define the continua via local spectral decompositions and show that the resulting approach converges independent of scales and contrast if representa-

---

* Corresponding author.
E-mail addresses: yalchinrefendiev@gmail.com, efendiev@math.tamu.edu (Y. Efendiev).
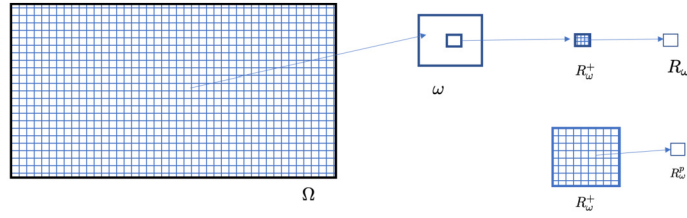
Fig. 1. Illustration.

tive volumes are chosen to be coarse blocks. In this work, we use similar ideas (as in [14,13,31]) for problems with scale separation and formulate cell problems and formally derive multicontinuum equations.

The main objectives of this paper are the following.

- We derive multicontinuum methods using a homogenization-like expansion and present constraint cell problem formulations.
- Constraint cell problems allow using averages for different quantities and regions (continua) and give flexibility to the framework.
- We discuss appropriate local boundary conditions in representative volume elements for problems with scale separation and introduce oversampling. Using oversampling, we consider reduced constraint cell problems, where we use constraints for the averages only.
- The resulting multicontinuum equations show that local averages of the solution will differ among each other if diffusion and reaction terms in the upscaled equations balance each other. This requires smaller reaction and/or larger diffusion terms, which occur in the presence of high contrast. We discuss this issue and show that a multicontinuum concept is via local spectral decomposition.
- We discuss the relation to NLMC approaches that go beyond scale separation.
- The average constraints, discussed in this paper, are easy to set and guarantee exponential decay (i.e., we remove boundary effects).
- We present numerical results.

We note that to go beyond scale separation, numerical approaches use entire coarse blocks (see Fig. 1) to do local computations [10,16–18,20,11,25]. Among these approaches, multiscale finite element method and its variations are proposed, where multiscale basis functions are computed on coarse grids.

1.1. The main idea of this paper

In this section, we briefly present the main idea of the paper. We consider a steady-state or dynamic problem

$$\mathcal{L}(u) = f$$

subject to some boundary and initial conditions. It is assumed that the problem is solved on a computational grid consisting of grid blocks, denoted ω, that are much larger than heterogeneities. We assume some type of homogeneity within each computational block represented by Representative Volume Element R_ω that corresponds to a computational element ω (see Fig. 1) (more precise meaning will be defined later). We assume that within each R_ω, there are several distinct average states can be achieved (known as multicontinua). We denote the characteristics function for continuum i within R_ω by ψ_i^ω (ω will be omitted since local computations are restricted to a coarse block), i.e., $\psi_i = 1$ within continuum i (can be irregular shaped regions consisting of several parts, in general) and 0 otherwise. We introduce oversampled R_ω^+ that contains several R_ω^p's. We denote the central (target) RVE by simply R_ω. In general, one can define the regions corresponding to the continuum via local spectral decomposition of the solution space within R_ω, as discussed later.

We assume a variational formulation of the problem

$$\sum_\omega \int_\omega \mathcal{A}(u, v) = \int_\Omega f v,$$

where $\mathcal{A}$ is the corresponding bilinear form. We assume that R_ω can be used to approximate each integral $\int_\omega$ (in general space-time integral). I.e.,

$$\int_\omega \mathcal{A}(u, v) \approx \frac{|\omega|}{|R_\omega|} \int_{R_\omega} \mathcal{A}(u, v). \tag{1}$$

Summation over repeated indices is assumed in the paper. Next, we construct local cell problems in R_ω that are used to represent u.

We assume there are several macroscopic quantities denoted by U_i^ω in each R_ω, where i is the continuum. These quantities can be thought of as average solutions within each continuum. We introduce cell problems in R_ω^+ (that consists of R_ω^p) that can distinguish these states. The first represents averages (formally written)

$$\mathcal{L}(\phi_i) = r_i \ \text{in} \ R_\omega^+$$
$$\sum_p \int_{R_\omega^p} \phi_i \psi_j^p = \delta_{ij} \int_{R_\omega^p} \psi_j^p, \tag{2}$$

where r_i accounts for constraints, ψ_j^p is ith continuum characteristics function in R_ω^p, and the second one accounts for the gradients (formally written)

$$\mathcal{L}(\phi_i^m) = r_i^m \ \text{in} \ R_\omega^+$$
$$\int_{R_\omega^p} \phi_i^m \psi_j^p = \delta_{ij} \int_{R_\omega^p} (x_m - c) \psi_j^p, \tag{3}$$

$$\int_{R_\omega^{p_0}} (x_m - c) \psi_j^{p_0} = 0 \ \text{(condition that defines } c\text{)}.$$

Additional initial conditions are posed. p_0 refers to the target RVE, R_ω. These cell problems are written formally and will more precisely be described in next sections. We will use oversampling regions and constraints in each RVE within an oversampled region to avoid boundary effects. Using these cell problems, the local solution in R_ω is written as

$$u \approx \phi_i U_i + \phi_i^m \nabla_m U_i. \tag{4}$$

We assume $U_i(x)$ is a smooth function representing the ith continuum. I.e., $U_i(x_\omega) \approx \int_{R_\omega} u \psi_i / \int_{R_\omega} \psi_i$, with x_ω being a center point of R_ω. Substituting (4) into (1) and taking $v \approx \phi_s V_s + \phi_s^k \nabla_k V_s$, we obtain multicontinuum equations for U_i. Substituting (4) and the form for v into equations, we obtain multicontinuum models.

We note that one can use $u = \widetilde{\phi}_i \widetilde{U}_i$ in deriving homogenized equations. In this case, $\widetilde{U}_i$ is a continuous function. Using proposed cell problems, we will have the first order approximation of $\widetilde{U}_i$ and, also, it paves a way to a higher order homogenization. We also note that $\nabla U_i \neq \int \nabla u \psi_i$ and this can be achieved using higher order homogenization. The convergence proof of our proposed approach will be presented elsewhere.

Our main contributions are the following.

- We formulate constrained cell problems using Lagrange multipliers.
- To avoid boundary effects, we formulate cell problems in oversampled regions and use solutions' averages to get fast decay of boundary effects. This is also shown numerically.
- We derive multicontinuum upscaled models and formulate scaling for each term, which is related to RVE size. This shows that unless there is some type of high contrast, the averages U_i within R_ω will become similar.
- We formulate spectral continuum definitions, which can be used to define ψ_i's.
- We discuss cell problems that use multiple constraints (averages and gradients) and discuss the advantages/disadvantages associated with such constraints.

The paper is organized as follows. In the next section, we present preliminaries and show the arguments used in [27]. Section 3 is devoted to the derivation of multicontinuum approaches for a scale separation case. In Section 4, we present spectral continuum ideas. Section 5 is devoted to some remarks that include the derivation using multiple constraints and nonlinear multicontinuum models. Finally, we present some numerical results in Section 6.

2. Preliminaries

2.1. The work of L. I. Rubinstein [27] from 1948

First, we briefly discuss the paper by L. I. Rubinstein [27], which is the first paper that derives multicontinuum equations based on physical laws. We skip/simplify some details. In [27], the author considers time-dependent diffusion equation in heterogeneous media. The equation at the fine scale is

$$u_t - \nabla \cdot (\kappa \nabla u) = f. \tag{5}$$

The paper [27] assumes that the media consists of many small particles (possible connected) divided into the group of N components (continua), where the diffusivity of each component is κ_i. The media is assumed to be stochastic, i.e., $\kappa(x, \zeta)$,

where ζ refers to a realization. At each point x, ω_x is an elementary volume around point x. We denote the distribution within a component i as $\widetilde{U}_i(x, t, \zeta)$ and denote by

$$U_i^*(x, t, \zeta) = \frac{1}{\omega_x} \int\limits_{\omega_x} \widetilde{U}_i(z, t, \zeta) dz$$

and denote (mathematical expectation)

$$U_i(x, t) = \int U_i^*(x, t, \zeta) d\nu(\zeta).$$

It is assumed that within a representative element, different components can have different averages and conservation for each component is written down. The conservation consists of three terms. The first term is the diffusion flux and is taken by (in [27])

$$q_{1i} = \int\limits_{\Sigma'} \kappa_i \frac{\partial U_i}{\partial n} \mu_i d\sigma \, \Delta t,$$

where μ_i is fraction of ith component on (larger) elementary volume boundary Σ', Δt is a time interval. There are a number of assumption about components' homogeneities on boundaries of Ω' (RVE). The second flux is taken to be heat exchange within an elementary volume, which occurs because of different temperatures within each component. Using Henry's law, this flux is written in [27] as

$$q_{2ij} = \int\limits_{\Omega'} \alpha_{ij}^*(U_j - U_{ij}) d\omega \Delta t,$$

where U_{ij} is a temperature in jth component when ith component temperature is U_i. It is taken to be $U_{ij} = U_i$. The third flux is given by

$$q_{3i} = \int\limits_{\Omega'} c_i \rho_i \frac{\partial U_i}{\partial t} p_i d\omega \Delta t,$$

where c_i, ρ_i represent fluid properties and p_i is a volume fraction of ith component. From

$$q_{3i} = q_{1i} + q_{2i}$$

one arrives to

$$\nabla \cdot (\kappa_i \mu_i \nabla U_i) + \sum_j \alpha_{ij}^*(U_j - U_i) = c_i \rho_i p_i \frac{\partial U_i}{\partial t}.$$

Similar multicontinuum models are proposed in different application areas.

In this paper, we give a derivation based on formal expansion, cell problems, and then show a relation to theories developed in [13,11]. This derivation can be made rigorous under some assumptions (cf. [12]). We mention some assumptions as we go along without making them formal to keep the presentation simple. Our derivation (1) reveals the nature of continua, (2) shows their relation to local spectral decomposition, and (3) formulate constraint cell problems with appropriate boundary conditions.

3. Multicontinuum derivation based on volume average constraints

3.1. Steady-state case

In this section, we will repeat some parts of Introduction. Our approach starts from a finite element method formulated on a coarse grid. Coarse grid contains RVE, where local computations will be performed (see Fig. 1). We assume a partition of the domain into elements, where ω is a generic coarse-grid element (triangle or rectangle), R_ω is a representative volume (RVE) within ω (see Fig. 1). We consider a steady state diffusion equation

$$\int\limits_\Omega \kappa \nabla u \cdot \nabla v = \int\limits_\Omega f v, \ v \in H_0^1(\Omega). \tag{6}$$

Representative volume, as usual, is assumed to represent the whole coarse block ω in terms of heterogeneities. In each R_ω, we assume N continua (components) and introduce

$\psi_j = 1$ in continuum j, 0 otherwise.

In general, one can use different functions, e.g., eigenfunctions of local problems [13,11] to represent each continuum, as discussed later.

Next, we remind that R_ω^+ is an oversampled region (RVE) that surrounds R_ω. It is taken to be several times larger compared to R_ω and consists of several RVE's, denoted by R_ω^p (p is the numbering). In general, they (R_ω^p's) can be the copies of R_ω and it is used to remove boundary effects. The target RVE, we denote by $R_\omega^{p_0}$ or simply R_ω. We introduce two sets of cell problems with constraints.

$$\int_{R_\omega^+} \kappa \nabla \phi_i^m \cdot \nabla v - \sum_{j,p} \frac{\beta_{ij}^{mp}}{\int_{R_\omega^p} \psi_j^p} \int_{R_\omega^p} \psi_j^p v = 0$$

$$\int_{R_\omega^p} \phi_i^m \psi_j^p = \delta_{ij} \int_{R_\omega^p} (x_m - c_{mj}) \psi_j^p, \tag{7}$$

$$\int_{R_\omega^{p_0}} (x_m - c_{mj}) \psi_j^{p_0} = 0 \text{ condition that defines } c,$$

where m refers to the coordinate direction, and

$$\int_{R_\omega^+} \kappa \nabla \phi_i \cdot \nabla v - \sum_{j,p} \frac{\beta_{ij}^p}{\int_{R_\omega^p} \psi_j^p} \int_{R_\omega^p} \psi_j^p v = 0$$

$$\int_{R_\omega^p} \phi_i \psi_j^p = \delta_{ij} \int_{R_\omega^p} \psi_j^p. \tag{8}$$

The first cell problem (7) one accounts for the gradient effects and is taken to vanish in the target RVE, $R_\omega^{p_0}$. This cell problem accounts for standard homogenization effects. The second cell problem (8) accounts for different averages in each continuum. By imposing the same averages in each R_ω^p, we reduce the boundary effects in an exponential manner [13,11]. Here, for simplicity, we do not use ω index in ϕ_i or ϕ_i^m, though both of them depend on ω. This is because our calculations will be done in each ω separately. In general, one can remove the index p in ψ_j if RVE's are periodically repeated or similar.

Next, we formulate some properties of β's. We note

$$\sum_{j,p} \beta_{ij}^p = 0 \tag{9}$$

which can be obtained by taking $v = 1$ in (32). If we take $v = \phi_k$ in (7), then, we have $\int_{R_\omega^+} \kappa \nabla \phi_i^m \cdot \nabla \phi_k = \sum_p \beta_{ik}^{mp}$. If we take $v = \phi_s$ in (8), we get

$$\beta_{is}^* = \int_{R_\omega^+} \kappa \nabla \phi_i \cdot \nabla \phi_s = \sum_p \beta_{is}^p. \tag{10}$$

We assume that in R_ω,

$$u \approx \phi_i U_i + \phi_i^m \nabla_m U_i, \tag{11}$$

where U_i is a smooth function representing the homogenized solution for ith continuum. More precisely, U_i can be thought as a limit of $\int_{R_\omega} u \psi_i / \int_{R_\omega} \psi_i$ (piecewise constant function) taken over all R_ω as the RVE size goes to zero. We will assume U_i and their gradients can be approximated by constants in RVE and use mid point to represent their values. We note that (11) can be shown under the assumption that U_i is a smooth function.

Next, we derive multicontinuum equations for U_i. For any $v \in H_0^1$, we have

$$\int_\Omega f v = \int_\Omega \kappa \nabla u \cdot \nabla v = \sum_\omega \int_\omega \kappa \nabla u \cdot \nabla v \approx \sum_\omega \frac{|\omega|}{|R_\omega|} \int_{R_\omega} \kappa \nabla u \cdot \nabla v, \tag{12}$$

where we make an assumption that integrated average over RVE can represent the whole computational element ω. This approximation holds if all $\int_{R_\omega^p}$ are approximately equal for all R_ω^p in ω. Next, we approximate each term

$$\int_{R_\omega} \kappa \nabla u \cdot \nabla v = \int_{R_\omega} \kappa \nabla (\phi_i U_i) \cdot \nabla v + \int_{R_\omega} \kappa \nabla (\phi_i^m \nabla_m U_i) \cdot \nabla v. \tag{13}$$

We assume that the variation of U_i and $\nabla_m U_i$ are small compared to the variations of ϕ_i and ϕ_i^m (see scalings (17)) and assume $\int_{R_\omega} \kappa \nabla(\phi_i U_i) \cdot \nabla v \approx \int_{R_\omega} \kappa (\nabla \phi_i) U_i \cdot \nabla v$ and $\int_{R_\omega} \kappa \nabla(\phi_i^m \nabla_m U_i) \cdot \nabla v \approx \int_{R_\omega} \kappa (\nabla \phi_i^m) \nabla_m U_i \cdot \nabla v$. We take

$$v = \phi_s V_s + \phi_s^k \nabla_k V_s.$$

Then, denoting for simplicity, $R_\omega = R_\omega^{p_0}$, we have

$$\int_{R_\omega} \kappa \nabla(\phi_i U_i) \cdot \nabla v \approx U_i(x_\omega) \int_{R_\omega} \kappa \nabla \phi_i \cdot \nabla v =$$

$$U_i(x_\omega) V_s(x_\omega) \int_{R_\omega} \kappa \nabla \phi_i \cdot \nabla \phi_s + U_i(x_\omega) \nabla_m V_s(x_\omega) \int_{R_\omega} \kappa \nabla \phi_i \cdot \nabla \phi_s^m = \tag{14}$$

$$U_i(x_\omega) \beta_{is}^* V_s(x_\omega) + \beta_{is}^{m*} U_i(x_\omega) \nabla V_s(x_\omega),$$

where

$$\beta_{ik}^{m*} = \int_{R_\omega} \kappa \nabla \phi_i^m \cdot \nabla \phi_k, \quad \beta_{ik}^* = \int_{R_\omega} \kappa \nabla \phi_i \cdot \nabla \phi_k.$$

Here, we use the fact that U_i and V_s are smooth functions and take their values at some points within ω. Similarly,

$$\int_{R_\omega} \kappa \nabla(\phi_i^m \nabla_m U_i) \cdot \nabla v \approx \nabla_m U_i(x_\omega) \int_{R_\omega^+} \kappa \nabla \phi_i^m \cdot \nabla v =$$

$$\nabla_m U_i(x_\omega) \nabla_k V_s(x_\omega) \int_{R_\omega} \kappa \nabla \phi_i^m \cdot \nabla \phi_s^k + \nabla_m U_i(x_\omega) V_s(x_\omega) \int_{R_\omega} \kappa \nabla \phi_i^m \cdot \nabla \phi_s \tag{15}$$

$$\nabla_m U_i(x_\omega) \nabla_k V_s(x_\omega) \alpha_{is}^{km} + \nabla_m U_i(x_\omega) V_s(x_\omega) \beta_{is}^{m*},$$

where

$$\alpha_{is}^{km} = \int_{R_\omega} \kappa \nabla \phi_i^m \cdot \nabla \phi_s^k.$$

Next, using continuous approximations for U_i and V_i, we can write

$$\int_{R_\omega} \kappa \nabla u \cdot \nabla v \approx U_i \beta_{ij}^{n*} \nabla_n V_j + U_i \beta_{ij}^* V_j +$$

$$\nabla_m U_i \alpha_{ij}^{mn} \nabla_n V_j + \nabla_m U_i \beta_{ij}^{m*} V_j. \tag{16}$$

Note that the definitions of α's and β's are using the volume of R_ω (which is of the same order as R_ω^+). Moreover, we also have the following scalings. Assume ϵ is a diameter of RVE. First, we note that

$$\|\phi_i\| = O(1), \ \|\nabla \phi_i\| = O(\frac{1}{\epsilon}) \tag{17}$$

$$\|\phi_i^m\| = O(\epsilon), \ \|\nabla \phi_i^m\| = O(1).$$

Using the formulas for α's and β's, we have the following scalings.

$$\beta_{ij}^{m*} = O(\frac{|R_\omega|}{\epsilon}), \ \alpha_{ij}^{mn} = O(|R_\omega|), \ \beta_{ij}^* = O(\frac{|R_\omega|}{\epsilon^2}).$$

We then define rescaled quantities $\widehat{\beta}_{ij}, \widehat{\alpha}_{ij}, \widehat{\beta}_{ij}, \widehat{\alpha}_{ij}$ such that

$$\widehat{\beta}_{ij}^{m*} = \frac{\epsilon}{|R_\omega|} \beta_{ij}^{m*}, \ \widehat{\alpha}_{ij}^{mn} = |R_\omega|^{-1} \alpha_{ij}^{mn} \ \widehat{\beta}_{ij} = \frac{\epsilon^2}{|R_\omega|} \beta_{ij}^*. \tag{18}$$

With these scalings, we have

$$\int_\Omega \kappa \nabla u \cdot \nabla v \approx \int_\Omega \widehat{\alpha_{ij}^{mn}} \nabla_m U_i \nabla_n V_j +$$

$$\frac{1}{\epsilon} \int_\Omega \widehat{\beta_{ij}^{m*}} \nabla_m U_i V_j + \frac{1}{\epsilon} \int_\Omega \widehat{\beta_{ij}^{m*}} U_i \nabla_m V_j + \frac{1}{\epsilon^2} \int_\Omega \widehat{\beta_{ij}} U_i V_j. \tag{19}$$

The sum of the second and third terms is negligible (this can be shown by integration by parts). It can be shown that

$$\sum_j \widehat{\beta_{ij}} \approx 0.$$

The last term can be written as

$$\int_\Omega \widehat{\beta_{ij}} U_i V_j = \sum_{j \neq i} \int_\Omega \widehat{\beta_{ij}} (U_i - U_j) V_j, \tag{20}$$

which gives a form that is often used in multicontinuum models. If we ignore the second and the third term in (19), we get

$$-\nabla_n(\widehat{\alpha_{ij}^{mn}} \nabla_m U_j) + \frac{1}{\epsilon^2} \widehat{\beta_{ij}} U_j = f_i \tag{21}$$

We see from the equation that the reaction term is dominant unless we deal with large diffusions (high contrast). When reaction terms dominate, we have all U_i's are approximately the same. Thus, in general, to define appropriate multicontinuum models (when U_i's differ), one needs appropriate multicontinuum definitions, which we will do in Section 4.

If we have one continuum (as in standard homogenization), then $\phi_1 = 1$ and $\beta_{ij}^p = 0$. The function ϕ_i^m will have the averages $\int_{R_\omega^p} \phi_1^m = \int_{R_\omega^p} (x_m - x_m^0)$, where $x_m^0 = \langle x_m \rangle_{R_\omega^{p0}}$. In this regard, ϕ_1^m acts as having linear growth as in homogenization case (see later discussions on imposing gradient constraints).

3.2. Time dependent case

We consider

$$\int_{t_n}^{t_{n+1}} \int_\Omega u_t v + \int_{t_n}^{t_{n+1}} \int_\Omega \kappa \nabla u \cdot \nabla v = \int_{t_n}^{t_{n+1}} \int_\Omega f v.$$

We introduce cell problems (we keep the same notations as the stationary case) as time-dependent cell problems in $R_\omega^+ \times [t_n, t_{n+1}]$

$$\int_{t_n}^{t_{n+1}} \int_{R_\omega^+} (\phi_i^m)_t v + \int_{t_n}^{t_{n+1}} \int_{R_\omega^+} \kappa \nabla \phi_i^m \cdot \nabla v -$$
$$\sum_p \frac{\beta_{ij}^{mp}}{\int_{t_n}^{t_{n+1}} \int_{R_\omega} \psi_j} \int_{t_n}^{t_{n+1}} \int_{R_\omega} \psi_j v = 0$$
$$\int_{t_n}^{t_{n+1}} \int_{R_\omega^p} \phi_i^m \psi_j = \delta_{ij} \int_{t_n}^{t_{n+1}} \int_{R_\omega^p} (x_m - c_{mj}) \psi_j \tag{22}$$
$$\int_{t_n}^{t_{n+1}} \int_{R_\omega^{p0}} (x_m - c_{mj}) \psi_j = 0$$
$$\phi_i^m(t = t_n) = \xi_i^m,$$

where ξ_i^m is the steady state solution given by (7). The second cell problem is defined with constraints on the average solutions in $R_\omega^+ \times [t_n, t_{n+1}]$

$$\int\limits_{t_n}^{t_{n+1}} \int\limits_{R_\omega^+} (\phi_i)_t v + \int\limits_{t_n}^{t_{n+1}} \int\limits_{R_\omega^+} \kappa \nabla \phi_i \cdot \nabla v -$$

$$\sum_p \frac{\beta_{ij}^p}{\int_{t_n}^{t_{n+1}} \int_{R_\omega} \psi_j} \int\limits_{t_n}^{t_{n+1}} \int\limits_{R_\omega} \psi_j v = 0 \tag{23}$$

$$\int\limits_{t_n}^{t_{n+1}} \int\limits_{R_\omega^p} \phi_i \psi_j = \delta_{ij} \int\limits_{t_n}^{t_{n+1}} \int\limits_{R_\omega^p} \psi_j$$

$$\phi_i(t = t_n) = \psi_i.$$

We again assume that in $R_\omega = R_\omega^{p_0}$

$$u \approx \phi_i U_i + \phi_i^m \nabla_m U_i. \tag{24}$$

Next, we derive multicontinuum equations for U_i. Then, we have (for any $v = \phi_s V_s + \phi_s^k \nabla_k V_s$)

$$\int\limits_{t_n}^{t_{n+1}} \int\limits_{\Omega} f v = \int\limits_{t_n}^{t_{n+1}} \int\limits_{\Omega} u_t v + \int\limits_{t_n}^{t_{n+1}} \int\limits_{\Omega} \kappa \nabla u \cdot \nabla v =$$

$$\sum_\omega \int\limits_{t_n}^{t_{n+1}} \int\limits_{\omega} u_t v + \sum_\omega \int\limits_{t_n}^{t_{n+1}} \int\limits_{\omega} \kappa \nabla u \cdot \nabla v \approx \tag{25}$$

$$\sum_\omega \frac{|\omega|}{|R_\omega|} \int\limits_{t_n}^{t_{n+1}} \int\limits_{R_\omega} u_t v + \sum_\omega \frac{|\omega|}{|R_\omega|} \int\limits_{t_n}^{t_{n+1}} \int\limits_{R_\omega} \kappa \nabla u \cdot \nabla v.$$

Next,

$$\int\limits_{t_n}^{t_{n+1}} \int\limits_{R_\omega} u_t v + \int\limits_{t_n}^{t_{n+1}} \int\limits_{R_\omega} \kappa \nabla u \cdot \nabla v \approx (U_i)_t V_k \int \int \phi_i \phi_k +$$

$$U_i V_k \int \int ((\phi_i)_t \phi_k + \kappa \nabla \phi_i \cdot \nabla \phi_k) + \nabla_m U_i \nabla_n V_k \int \int ((\phi_i^m)_t \phi_k^n + \kappa \nabla \phi_i^m \cdot \nabla \phi_k^n) +$$

$$U_i \nabla_n V_k \int \int ((\phi_i)_t \phi_k^n + \kappa \nabla \phi_i \cdot \nabla \phi_k^n) + \nabla_m U_i V_k \int \int ((\phi_i^m)_t \phi_k + \kappa \nabla \phi_i^m \cdot \nabla \phi_k) + \tag{26}$$

$$(U_i)_t \nabla_n V_k \int \int \phi_i \phi_k^n = m_{ik} (U_i)_t V_k + \beta_{ik} U_i V_k + \alpha_{ij}^{nm} \nabla_m U_i \nabla_n V_k +$$

$$\beta_{ik}^n U_i \nabla_n V_k + \alpha_{ik}^m \nabla_m U_i V_k + m_{ij}^n (U_i)_t \nabla_n V_k.$$

We note that if the cell problems do not contain t, i.e., ϕ_i^m and ϕ_i do not depend on t, we get similar homogenized equations (which can easily be derived from (26)). Here for simplicity of the notations, $\int \int \cdot = \int_{t_n}^{t_{n+1}} \int_{R_\omega} \cdot$ and the notations for m_{ik}, β_{ik}, α_{ij}^{nm}, β_{ik}^n, α_{ik}^m, and m_{ij}^n can be seen from the above equality. We neglect $\phi_i^m \nabla_m U_i$ and $(U_i)_t \nabla_n V_k \int \int \phi_i \phi_k^n$ based on scalings (27).

Assume ϵ is a diameter of RVE. We note that

$$\|\phi_i\| = O(1), \ \|\nabla \phi_i\| = O(\frac{1}{\epsilon}) \tag{27}$$

$$\|\phi_i^m\| = O(\epsilon), \ \|\nabla \phi_i^m\| = O(1).$$

Thus, the last term in (26) can be neglected.

Using continuous approximation U_i's and V_i's, we can write

$$
\int_{t_n}^{t_{n+1}} \int_{\Omega} f v = \int_{t_n}^{t_{n+1}} \int_{\Omega} u_t v + \int_{t_n}^{t_{n+1}} \int_{\Omega} \kappa \nabla u \cdot \nabla v \approx
$$

$$
\int_{t_n}^{t_{n+1}} \int_{\Omega} \widetilde{m_{ij}}(U_i)_t V_j + \int_{t_n}^{t_{n+1}} \int_{\Omega} \widetilde{\alpha_{ij}^{mn}} \nabla_m U_i \nabla_n V_j +
$$

$$
\int_{t_n}^{t_{n+1}} \int_{\Omega} \widetilde{\alpha_{ij}^{m}} \nabla_m U_i V_j + \int_{t_n}^{t_{n+1}} \int_{\Omega} \widetilde{\beta_{ij}^{n}} U_i \nabla_n V_j +
$$

$$
\int_{t_n}^{t_{n+1}} \int_{\Omega} \widetilde{\beta_{ij}} U_i V_j, \tag{28}
$$

where $\widetilde{\cdot}$ denotes rescaled $\cdot$ with scaling of R_ω and Δt (i.e., $\widetilde{\cdot} = \frac{\cdot}{|R_\omega||\Delta t|}$ so that we can write the integrals.

Formally, we can write the system of differential equations

$$
(U_i)_t - \nabla_n \widetilde{\alpha_{ij}^{mn}} \nabla_m U_j + \widetilde{\beta_{ij}^{m}} \nabla_m U_j
$$
$$
- \nabla_n (\widetilde{\alpha_{ij}^{n}} U_j) + \widetilde{\beta_{ij}} U_j = f_i \tag{29}
$$

Using the formulas for α's and β's, we have the following scalings (if we ignore the terms with temporal derivatives)

$$
\beta_{ij}^{m} = O(\frac{|R_\omega|\Delta t}{\epsilon}), \alpha_{ij}^{mn} = O(|R_\omega|\Delta t)
$$

$$
\beta_{ij} = O(\frac{|R_\omega|\Delta t}{\epsilon^2}), \alpha_{ij}^{n} = O(\frac{|R_\omega|\Delta t}{\epsilon}).
$$

One can make similar argument as in steady state case.

4. Choices of continua. Spectral continua

In this section, we discuss how high contrast can balance α's and β's. First, we note that if reaction terms (represented via β) dominate, then all U_i's are approximately the same and we do not have multicontinuum (i.e., different averages in different continua). We assume steady-state case and two continua, where the continuum 1 has high-contrast $\kappa = O(\eta)$, η is large, and the continuum 2 has a conductivity of order 1. The next arguments do not take into account RVE sizes and are purely in terms of η. We can see that α_{is}^{km} (the diffusivity) is large $O(\eta)$ (at least in some direction) since the local solutions have linear growth conditions. In general, the scalings of α's in terms of the contrast depend on heterogeneities (see numerical results). On the other hand, β_{11} is of order 1 (in terms of the contrast, while it depends on the size of R_ω). Since $\sum_j \beta_{ij} \approx 0$, we can conclude that other β's are of order 1. Thus, if the contrast balances the RVE size (e.g., $\eta = O(\epsilon^{-2})$) (where ϵ is the size of R_ω), we expect that β terms do not dominate and there are differences between average states and one has multicontinuum homogenized limit.

Next, we discuss how one can identify the continuum via local spectral problems. We consider $\beta_{ij} = \int_{R_\omega} \kappa \nabla \phi_i \cdot \nabla \phi_j$ and assume, for simplicity, that the cell problem (8) is formulated in R_ω. We would like to minimize β_{ij} with constraints. We assume (1) ϕ_i's are in the space of local solutions (ζ_j) (2) ψ_j can take any values and the constraints are given by $\int_{R_\omega} \kappa \phi_i \psi_j = \delta_{ij}$. The functions ζ_j are local homogeneous solutions, $\nabla \cdot (\kappa \nabla \zeta_j) = 0$ in R_ω, with boundary conditions $\zeta_j = \delta_j^h(x)$ on ∂R_ω, where $\delta_j(x)$ is a fine-grid hat function defined on the boundary of R_ω. In this case, if we consider the eigenvalue problem

$$
-div(\kappa \nabla \eta_j) = \lambda_j \kappa \eta_j. \tag{30}
$$

(see [16,11]). With corresponding Rayleigh quotient,

$$
\frac{\int_{R_\omega} \kappa |\nabla \phi|^2}{\int_{R_\omega} \kappa |\phi|^2},
$$

it is clear that $\psi_j = \phi_j = \eta_j$. The eigenvectors corresponding to the smallest eigenvalues are constant functions in high-contrast regions. In general, one can identify high-contrast regions by finding nearly constant gradient regions of $\nabla \phi_j$.

Moreover, the number of smallest eigenvalues will correspond to the number of high-conductivity channels (channels that connect boundaries of R_ω).

Based on the above discussion, one can perform local spectral decomposition based on (30) and identify ψ_j based on smallest eigenvalues that correspond to high contrast (they scale as the inverse of high contrast). Using these eigenvectors, the local problems (8) and (7) are solved. We can use instead of $\beta_{ij}^{mp} / \int_{R_\omega^p} \psi_j^p$ and $\beta_{ij}^p / \int_{R_\omega^p} \psi_j^p$, the terms without denominator, β_{ij}^{mp} and β_{ij}^p so that not to worry that ψ_j^p may vanish.

5. Remarks

5.1. Multicontinuum derivation based on average and gradient constraint problems in representative volumes

One can also use gradient type constraints in addition. We demonstrate this and point out some issues in this procedure. We consider a steady state diffusion equation.

In each RVE, we introduce two sets of cell problems with constraints formulated in R_ω (though, one can use oversampling).

$$
\int_{R_\omega} \kappa \nabla \phi_i^m \cdot \nabla v - \frac{\alpha_{ij}^{mn}}{\int_{R_\omega} \psi_j} \int_{R_\omega} \psi_j \nabla_n v - \frac{\beta_{ij}^m}{\int_{R_\omega} \psi_j} \int_{R_\omega} \psi_j v = 0
$$

$$
\int_{R_\omega} \nabla \phi_i^m \psi_j = \delta_{ij} e_m \int_{R_\omega} \psi_j
$$

$$
\int_{R_\omega} \phi_i^m \psi_j = 0,
$$

(31)

where e_m is mth unit vector. The second cell problem is defined with constraints on the average solutions in R_ω

$$
\int_{R_\omega} \kappa \nabla \phi_i \cdot \nabla v - \frac{\alpha_{ij}^n}{\int_{R_\omega} \psi_j} \int_{R_\omega} \psi_j \nabla_n v - \frac{\beta_{ij}}{\int_{R_\omega} \psi_j} \int_{R_\omega} \psi_j v = 0
$$

$$
\int_{R_\omega} \phi_i \psi_j = \delta_{ij} \int_{R_\omega} \psi_j
$$

$$
\int_{R_\omega} \nabla \phi_i \psi_j = 0.
$$

(32)

Some properties of Lagrange multipliers are discussed. We note $\sum_j \beta_{ij} = 0$, which can be obtained by taking $v = 1$ in (32). If we take $v = \phi_j$ in (31) then $\int_{R_\omega} \kappa \nabla \phi_i^m \cdot \nabla \phi_j = \beta_{ij}^m$. If we take $v = \phi_k^m$ in (32), we get $\int_{R_\omega} \kappa \nabla \phi_i \cdot \nabla \phi_k^m = \alpha_{ik}^m$. Therefore, $\alpha_{ij}^m = \beta_{ij}^m$. If we take $v = \phi_k^s$ in (31), then, we have $\int_{R_\omega} \kappa \nabla \phi_i^m \cdot \nabla \phi_k^s = \alpha_{ik}^{ms}$. If we take $v = \phi_s$ in (32), we get $\int_{R_\omega} \kappa \nabla \phi_i \cdot \nabla \phi_s = \beta_{is}$.

Next, we assume that the local solution in ω can be represented by constraint problems in R_ω

$$
u \approx \phi_i U_i + \phi_i^m V_i^m,
$$

(33)

where

$$
U_i = \frac{\int_{R_\omega} u \psi_i}{\int_{R_\omega} \psi_i}, \quad V_i^m = \frac{\int_{R_\omega} \nabla_m u \psi_i}{\int_{R_\omega} \psi_i}.
$$

(34)

Similarly, we introduce for test functions

$$
P_i = \frac{\int_{R_\omega} v \psi_i}{\int_{R_\omega} \psi_i}, \quad Q_i^m = \frac{\int_{R_\omega} \nabla_m v \psi_i}{\int_{R_\omega} \psi_i}.
$$

(35)

For any $v \in H_0^1$, we have

$$
\int_\Omega f v = \int_\Omega \kappa \nabla u \cdot \nabla v = \sum_\omega \int_\omega \kappa \nabla u \cdot \nabla v \approx \sum_\omega \frac{|\omega|}{|R_\omega|} \int_{R_\omega} \kappa \nabla u \cdot \nabla v,
$$

(36)

where we make an assumption that integrated average over RVE can represent the whole computational element ω. Next, we approximate each term

$$\int_{R_\omega} \kappa \nabla u \cdot \nabla v = \int_{R_\omega} \kappa \nabla(\phi_i U_i) \cdot \nabla v + \int_{R_\omega} \kappa \nabla(\phi_i^m V_i^m) \cdot \nabla v. \tag{37}$$

We assume that the variation of U_i and V_i^m are small compared to the variations of ϕ_i and ϕ_i^m (since they vary at RVE scale) and assume $\int_{R_\omega} \kappa \nabla(\phi_i U_i) \cdot \nabla v \approx \int_{R_\omega} \kappa(\nabla \phi_i) U_i \cdot \nabla v$ and $\int_{R_\omega} \kappa \nabla(\phi_i^m V_i^m) \cdot \nabla v \approx \int_{R_\omega} \kappa \nabla(\phi_i^m) V_i^m \cdot \nabla v$. Then (denoting x_ω center of R_ω),

$$\int_{R_\omega} \kappa \nabla(\phi_i U_i) \cdot \nabla v \approx U_i(x_\omega) \int_{R_\omega} \kappa \nabla \phi_i \cdot \nabla v =$$

$$U_i(x_\omega) \frac{\alpha_{ij}^n}{\int_{R_\omega} \psi_j} \int_{R_\omega} \psi_j \cdot \nabla_n v + U_i(x_\omega) \frac{\beta_{ij}}{\int_{R_\omega} \psi_j} \int_{R_\omega} \psi_j v = \tag{38}$$

$$U_i(x_\omega) \alpha_{ij}^n Q_j^n(x_\omega) + U_i(x_\omega) \beta_{ij} P_j(x_\omega).$$

Similarly,

$$\int_{R_\omega} \kappa \nabla(\phi_i^m \nabla_m U_i) \cdot \nabla v \approx V_i^m(x_\omega) \int_{R_\omega} \kappa \nabla \phi_i^m \cdot \nabla v =$$

$$\frac{\alpha_{ij}^{mn}}{\int_{R_\omega} \psi_j} V_i^m(x_\omega) \int_{R_\omega} \psi_j \nabla_n v + \frac{\beta_{ij}^m}{\int_{R_\omega} \psi_j} V_i^m(x_\omega) \int_{R_\omega} \psi_j v = \tag{39}$$

$$V_i^m(x_\omega) \alpha_{ij}^{mn} Q_j^n(x_\omega) + V_i^m(x_\omega) \beta_{ij}^m P_j(x_\omega).$$

Next, using continuous approximations for all quantities, we have

$$\int_{R_\omega} \kappa \nabla u \cdot \nabla v \approx U_i \alpha_{ij}^n Q_j^n + U_i \beta_{ij} P_j +$$

$$V_i^m \alpha_{ij}^{mn} Q_j^n + V_i^m \beta_{ij}^m P_j. \tag{40}$$

Consequently,

$$\int_\Omega f v = \int_\Omega \kappa \nabla u \nabla v \approx \int_\Omega \widetilde{\alpha_{ij}^{mn}} V_i^m Q_j^n +$$

$$\int_\Omega \widetilde{\beta_{ij}^m} V_i^m P_j + \int_\Omega \widetilde{\alpha_{ij}^n} U_i Q_j^n + \int_\Omega \widetilde{\beta_{ij}} U_i P_j, \tag{41}$$

where $\widetilde{\cdot}$ denotes rescaled $\cdot$ with scaling (i.e., $\widetilde{\cdot} = \frac{\cdot}{|R_\omega|}$). The equation (41) is a multicontinuum model equation. Similar scaling arguments as before can be applied.

The resulting equations are similar to those we obtained earlier. In our numerical studies, we have found that the cell problems using multiple simultaneous constraints (e.g., average solution and average gradient) are prone to large errors. This is because one needs to choose these simultaneous constraints (for averages and gradients) such that the local problems ϕ_i and ϕ_i^m have similar fine-scale features as the exact solution. When there is no compatibility (i.e., averages and gradients do not correspond to each other), then there are large errors, especially at the interfaces of the continuum, which can cause large errors on average characteristics. For this reason, we have found one constraint cell problems to be more accurate, easy to implement, and easy to remove boundary effects with oversampling.

5.2. Nonlinear case. Steady state

The derivations presented earlier can be done for nonlinear problems. We consider

$$\int_\Omega \kappa(x, \nabla u) \cdot \nabla v = \int_\Omega f v.$$

In this case, we can split the cell problem into average-based and gradient based due to nonlinear interaction and we consider the following cell problem.

$$\int_{R_\omega^+} \kappa(x, \nabla\phi(\eta, \xi)) \cdot \nabla v - \sum_p \alpha_\omega^{p,j}(\eta, \xi) \int_{R_\omega^p} \psi_j^p v = 0$$

$$\int_{R_\omega^p} \phi^{\eta,\xi} \psi_j^p = \eta_j \int_{R_\omega^p} \psi_j^p + \xi_j \cdot \int_{R_\omega^p} (x - c) \psi_j^p. \tag{42}$$

We will use the following approximations

$$u \approx \phi(U, \nabla U)$$

$$v|_{R_\omega^p} \approx \sum_i V_i \frac{\psi_i^p}{\int \psi_i^p} + \sum_i \frac{\psi_i^p}{\int \psi_i^p}(x - c_i) \cdot \nabla V_i.$$

Then,

$$\int_{R_\omega^+} \kappa(x, \nabla\phi(U, \nabla U)) \cdot \nabla v = \sum_p \alpha_\omega^{p,j}(U, \nabla U) V_i \frac{\int_{R_\omega^p} \psi_j^p \psi_i^p}{\int_{R_\omega^p} |\psi_i^p|^2} +$$

$$\sum_p \alpha_\omega^{p,j}(U, \nabla U) \frac{\int_{R_\omega^p} \psi_j^p \psi_i^p(x - c_i)}{\int_{R_\omega^p} \psi_i^p} \cdot \nabla V_i = \tag{43}$$

$$\sum_p \alpha_\omega^{p,j}(U, \nabla U) V_j + \sum_{m,p} \beta^{jm}(U, \nabla U) \nabla_m V_j,$$

where all U's and V's are taken to be constants at RVE-level and

$$\gamma^j(\eta, \xi) = \sum_p \alpha_\omega^{p,j}(\eta, \xi)$$

$$\beta^{jm}(\eta, \xi) = \sum_p \alpha_\omega^{p,j}(\eta, \xi) \frac{\int_{R_\omega^p} (x_m - c_m) \psi_j^p}{\int \psi_j^p}.$$

Here, we took account $\int_{R_\omega^p} \psi_j^p \psi_i^p = \delta_{ij} \int_{R_\omega^p} \psi_i^p$ and $\int_{R_\omega^p} \psi_j^p \psi_i^p(x - c_i) = \delta_{ij} \int_{R_\omega^p} \psi_i^p(x - c_i)$. We get the following multicontinuum equations

$$\int_\Omega \gamma^j(U, \nabla U) V_j + \int_\Omega \beta^j(U, \nabla U) \cdot \nabla V_j = f_j.$$

In general, these equations are complicated to solve. Some machine learning techniques are needed to train the local upscaled quantities. We have presented some cases in [22,29,14]. In some special cases, one can simplify the resulting multicontinuum equations.

6. Numerical results

In this section, we will present numerical examples of the proposed upscaling method. We will present three numerical examples. The goal is to show that our proposed algorithm is accurate and the cell problem solutions provide better accuracy as we increase oversampling size.

In all examples, we consider the elliptic problem (6) in a unit square, and solve the cell problems (7) and (8). The macroscopic equation is given by (21). In the first example, we consider the layered medium parameter κ (see Fig. 2). The period of κ is denoted as ϵ. We denote the low conductivity region and the high conductivity region of κ by Ω_1 and Ω_2, respectively. The source term f and conductivity κ is given as

$$f(x) = \begin{cases} 1000 \min\{\kappa\} e^{-40|(x-0.5)^2 + (y-0.5)^2|} & x \in \Omega_1 \\ e^{-40|(x-0.5)^2 + (y-0.5)^2|} & x \in \Omega_2 \end{cases}$$

and

$$\kappa(x) = \begin{cases} \dfrac{\epsilon}{10000} & x \in \Omega_1 \\ \dfrac{1}{100\epsilon} & x \in \Omega_2 \end{cases}$$
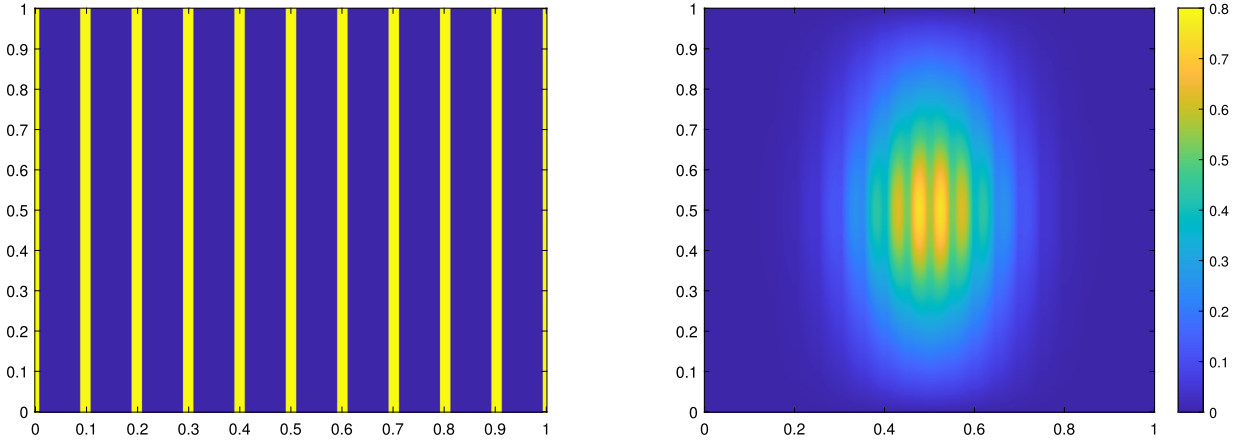
Fig. 2. Left: κ for Case 1 with $\epsilon = \dfrac{1}{10}$. Right: The solution snapshot.

The computational domain Ω is partitioned into $M \times M$ coarse grid. The coarse mesh size H is defined as $H = 1/M$. For simplicity, we consider the whole coarse grid element as an RVE for the corresponding coarse element. The oversampling RVE R_ω^+ (or ω^+) for each coarse RVE ω is defined as an extension of K by l layers of coarse grid element, where l will be varied.

We will define the relative L^2-error in Ω_1 and the relative L^2-error in Ω_2 by

$$
e_2^{(i)} = \frac{\sum_K |\frac{1}{|K|} \int_K U_i - \frac{1}{|K \cap \Omega_i|} \int_{K \cap \Omega_i} u|^2}{\sum_K |\frac{1}{K \cap \Omega_i} \int_{K \cap \Omega_i} u|^2}.
$$

K denotes the RVE, which is taken to be ω. This represents the L_2 error of our proposed approach.

Our goals in this section are the following.

- We show that the errors between the upscaled solutions and corresponding fine-grid solutions are small.
- The errors are stable for different mesh sizes, RVE sizes, and contrasts. If the number of layers is appropriately chosen (to avoid boundary effects), the error will decrease as we decrease the mesh size.
- We discuss the effective properties and show their values for different values of mesh sizes and RVE sizes.
- The numerical results show scalings of effective parameters.

For the first case, we take the fine-mesh size to be $1/800$. We present $e_2^{(i)}$ in Table 1. We make several observations. First, we observe that the proposed approach provides an accurate approximation of the averaged solution. In Fig. 3, we depict upscaled solutions and corresponding averaged fine-scale solutions. We observe that these solutions are very close. In the first table, we decrease the coarse-mesh size and it gets closer to ϵ. In standard numerical homogenization methods, this was known to give a resonance error and error will increase. Here, by choosing an appropriate number of layers, we observe that the error remains small. In the second table, we decrease the period size and observe that the error decreases to a certain level. In the third table, we observe convergence as we decrease the mesh size and ϵ. In general, we expect a certain threshold error due to fine-scale discretization, which is used to compute the solution. In Table 2, we present the errors for fixed contrast ratio $1/10000$ (in Ω_1) and $1/10$ (in Ω_2). As we decrease the mesh and RVE sizes, we observe that the upscaled solution converges to the averaged fine-scale solution.

In Table 3, we present the results for effective properties that are computed. First, we note that the scalings of these quantities are in accordance with our theoretical findings. In Case 1, we observe anisotropy as expected. $\alpha_{11}^{mn} \approx 0$, unless $i = j = 2$ since the flow in vertical direction for the gradient. We observe larger α_{22}^{22} since the flow in the vertical direction and the second continuum accounts for high conductivity. We only show β_{11} as other β_{ij}'s depend on them and are similar (follows from symmetry and the fact that the sum of elements in each row is zero). We note that with our scalings of conductivity, β should scale as $1/\epsilon$, which we observe in the table.

6.1. Case 2

Next, we consider a different case, Case 2. We depict the conductivity field in Fig. 4 and the corresponding fine-grid solution. The fine-mesh size is taken to be $1/400$. In Fig. 5, we depict upscaled solutions and corresponding averaged fine-
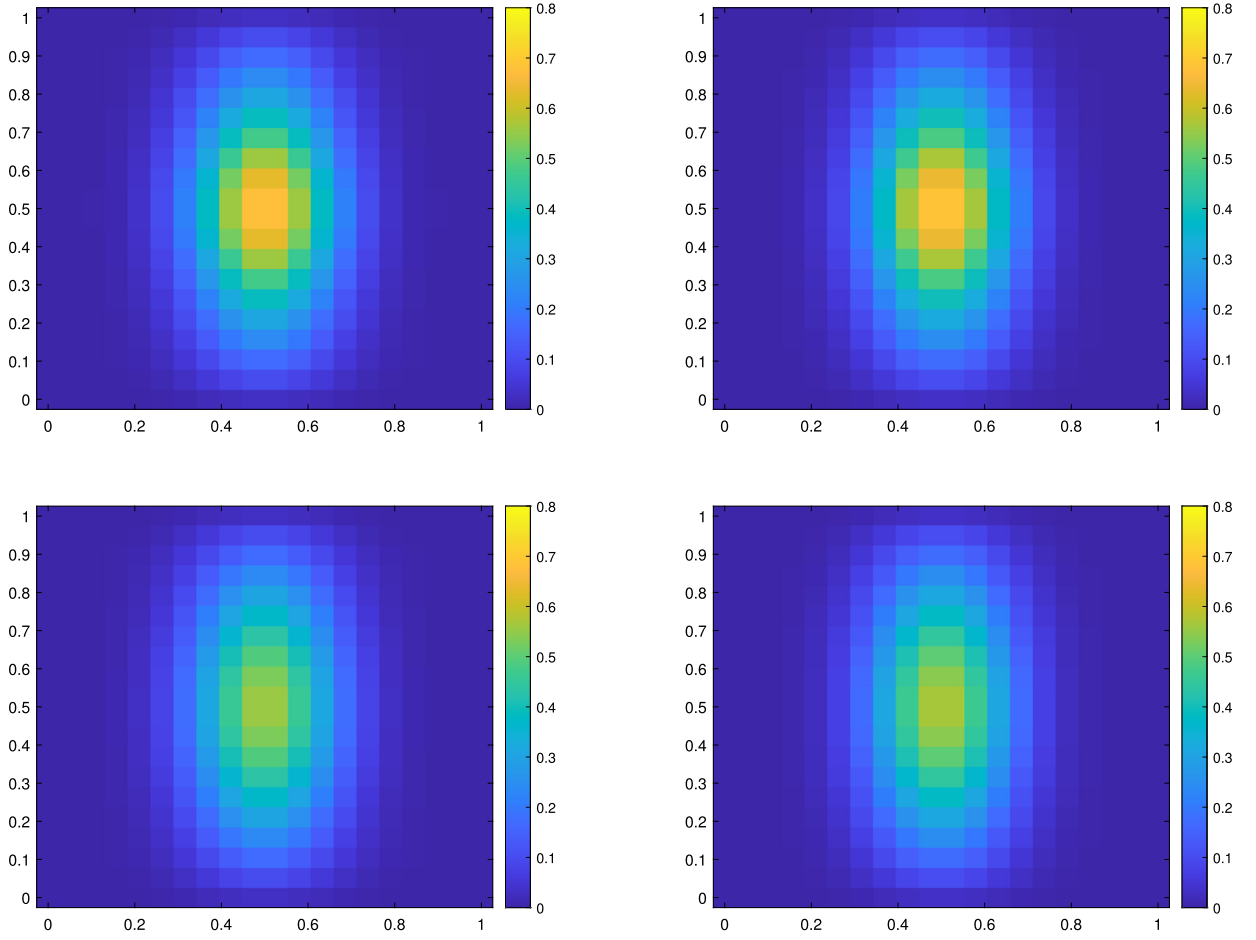
Fig. 3. Case 1. Top-Left: Reference averaged solution in Ω_1. Top-Right: Multiscale solution U_1. Bottom-Left: Reference averaged solution in Ω_2. Bottom-Right: Multiscale solution U_2.

scale solutions. We observe that these solutions are very close. For this case, we present $e_2^{(i)}$ in Table 4. We observe similar findings. First, we observe that the proposed approach provides an accurate approximation of the averaged solution. In this table, we decrease the coarse mesh size while keeping ϵ fixed. We observe that the error decreases if we scale the number of layers as $-\log(H)$. In the second part of the table, we decrease ϵ and observe that error does not change if the number of layers is fixed. Finally, we reduce both H and ϵ and observe that the error decreases. Thus, the proposed method is robust with respect to the size of heterogeneities.

In Table 5, numerical results for effective properties are presented. In this case, we do not have strong anisotropy and observe similar values for α's when the continua are fixed. From the second table, we observe that the values of α_{22}^{mn} are larger compared to α_{11}^{mn} and α_{12}^{mn}. This is because the second continuum account for high conductivity region. Again, β should scale as $1/\epsilon$, which we observe in the table.

6.2. Case 3

Next, we consider a different case, Case 3. We depict the conductivity field in Fig. 6 and corresponding fine-grid solution. In this case, we do not have strict periodicity as in other cases and the conductivity slowly changes. The fine-mesh size is taken to be $1/400$. In Fig. 7, we depict upscaled solutions and corresponding averaged fine-scale solutions. We observe that these solutions are approximately the same. For this case, we present $e_2^{(i)}$ in Table 6. We observe similar findings as in previous cases. First, we observe that the proposed approach provides an accurate approximation of the averaged solution. In this table, we decrease the coarse mesh size while keeping ϵ fixed. We observe that the error decreases if we scale the number of layers as $-\log(H)$. In the second part of the table, we decrease ϵ and observe that error does not change if the number of layers is fixed. Finally, we reduce both H and ϵ and observe that the error decreases. Thus, the proposed method is robust with respect to the size of heterogeneities.

Table 1
Error comparison for Case 1.

l	H	ϵ	$e_2^{(1)}$	$e_2^{(2)}$
$\lceil -2\log(H) \rceil = 5$	$\dfrac{1}{10}$	$\dfrac{1}{40}$	1.50%	1.37%
$\lceil -2\log(H) \rceil = 6$	$\dfrac{1}{20}$	$\dfrac{1}{40}$	0.48%	0.50%
$\lceil -2\log(H) \rceil = 8$	$\dfrac{1}{40}$	$\dfrac{1}{40}$	0.61%	0.60%

l	H	ϵ	$e_2^{(1)}$	$e_2^{(2)}$
5	$\dfrac{1}{10}$	$\dfrac{1}{10}$	4.60%	8.35%
5	$\dfrac{1}{10}$	$\dfrac{1}{20}$	1.60%	1.31%
5	$\dfrac{1}{10}$	$\dfrac{1}{40}$	1.50%	1.37%

l	H	ϵ	$e_2^{(1)}$	$e_2^{(2)}$
$\lceil -2\log(H) \rceil = 5$	$\dfrac{1}{10}$	$\dfrac{1}{10}$	4.60%	8.35%
$\lceil -2\log(H) \rceil = 6$	$\dfrac{1}{20}$	$\dfrac{1}{20}$	2.02%	2.40%
$\lceil -2\log(H) \rceil = 8$	$\dfrac{1}{40}$	$\dfrac{1}{40}$	0.61%	0.60%
$\lceil -2\log(H) \rceil = 9$	$\dfrac{1}{80}$	$\dfrac{1}{80}$	0.14%	0.14%

Table 2
Error comparison for Case 1 with a fixed contrast.

l	H	ϵ	$e_2^{(1)}$	$e_2^{(2)}$
$\lceil -2\log(H) \rceil = 5$	$\dfrac{1}{10}$	$\dfrac{1}{10}$	3.83%	6.24%
$\lceil -2\log(H) \rceil = 6$	$\dfrac{1}{20}$	$\dfrac{1}{20}$	2.20%	2.50%
$\lceil -2\log(H) \rceil = 8$	$\dfrac{1}{40}$	$\dfrac{1}{40}$	0.88%	0.90%
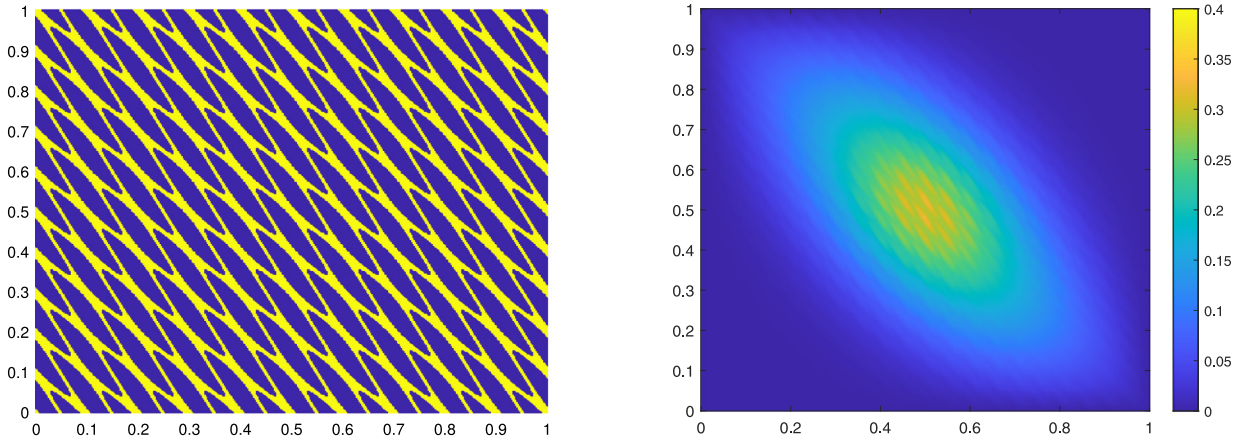
Fig. 4. Left: κ for Case 2 with $\epsilon = \dfrac{1}{10}$. Right: The solution snapshot.

7. Conclusions

In this paper, we propose a derivation of multicontinuum models using constraint cell problems in oversampled regions. The proposed cell problems allow reducing boundary effects and take into account both average and gradient constraints. Imposing constraints on averages allows a fast decay of artificial boundary effects. Our derivations show that one obtains coupled equations and derives the formula for exchange between continua. The exchange terms in the form of the reaction scale as the square of the inverse of RVE size and, thus, they dominate. As a result, the solutions in these continua are equal

**Table 3**
Effective properties α and β's. Case 1.

l	H	ϵ	$\alpha_{11}^{11}/|R_\omega|$	$\alpha_{11}^{21}/|R_\omega|$	$\alpha_{11}^{22}/|R_\omega|$
$\lceil -2\log(H)\rceil = 5$	$\frac{1}{10}$	$\frac{1}{10}$	≈ 0	≈ 0	1.9685e-05
$\lceil -2\log(H)\rceil = 5$	$\frac{1}{10}$	$\frac{1}{20}$	≈ 0	≈ 0	1.9006e-05
$\lceil -2\log(H)\rceil = 5$	$\frac{1}{10}$	$\frac{1}{40}$	≈ 0	≈ 0	1.9247e-05

l	H	ϵ	$\alpha_{22}^{11}/|R_\omega|$	$\alpha_{22}^{21}/|R_\omega|$	$\alpha_{22}^{22}/|R_\omega|$
$\lceil -2\log(H)\rceil = 5$	$\frac{1}{10}$	$\frac{1}{10}$	1.4876e-05	≈ 0	0.0201
$\lceil -2\log(H)\rceil = 5$	$\frac{1}{10}$	$\frac{1}{20}$	6.2843e-06	≈ 0	0.0401
$\lceil -2\log(H)\rceil = 5$	$\frac{1}{10}$	$\frac{1}{40}$	3.1331e-06	≈ 0	0.0802

l	H	ϵ	$\alpha_{12}^{11}/|R_\omega|$	$\alpha_{12}^{12}/|R_\omega|$	$\alpha_{12}^{22}/|R_\omega|$
$\lceil -2\log(H)\rceil = 5$	$\frac{1}{10}$	$\frac{1}{10}$	≈ 0	≈ 0	-1.1669e-05
$\lceil -2\log(H)\rceil = 5$	$\frac{1}{10}$	$\frac{1}{20}$	≈ 0	≈ 0	-1.4998e-05
$\lceil -2\log(H)\rceil = 5$	$\frac{1}{10}$	$\frac{1}{40}$	≈ 0	≈ 0	-1.7243e-05

| l	H	ϵ	$\beta_{11}/|R_\omega|$	$\beta_{12}/|R_\omega|$	$\beta_{22}/|R_\omega|$
$\lceil -2\log(H)\rceil = 5$	$\frac{1}{10}$	$\frac{1}{10}$	0.0150	-0.0150	0.0150
$\lceil -2\log(H)\rceil = 5$	$\frac{1}{10}$	$\frac{1}{20}$	0.0301	-0.0301	0.0301
$\lceil -2\log(H)\rceil = 5$	$\frac{1}{10}$	$\frac{1}{40}$	0.0610	-0.0610	0.0610

Table 4
Error comparison for Case 2.

l	H	ϵ	$e_2^{(1)}$	$e_2^{(2)}$
$\lceil -2\log(H)\rceil = 5$	$\frac{1}{10}$	$\frac{1}{40}$	8.42%	8.54%
$\lceil -2\log(H)\rceil = 6$	$\frac{1}{20}$	$\frac{1}{40}$	2.42%	2.50%
$\lceil -2\log(H)\rceil = 8$	$\frac{1}{40}$	$\frac{1}{40}$	0.65%	0.72%

l	H	ϵ	$e_2^{(1)}$	$e_2^{(2)}$
5	$\frac{1}{10}$	$\frac{1}{10}$	8.28%	10.08%
5	$\frac{1}{10}$	$\frac{1}{20}$	9.60%	10.17%
5	$\frac{1}{10}$	$\frac{1}{40}$	8.42%	8.54%

l	H	ϵ	$e_2^{(1)}$	$e_2^{(2)}$
$\lceil -2\log(H)\rceil = 5$	$\frac{1}{10}$	$\frac{1}{10}$	8.28%	10.08%
$\lceil -2\log(H)\rceil = 6$	$\frac{1}{20}$	$\frac{1}{20}$	2.98%	3.43%
$\lceil -2\log(H)\rceil = 8$	$\frac{1}{40}$	$\frac{1}{40}$	0.65%	0.72%
$\lceil -2\log(H)\rceil = 9$	$\frac{1}{80}$	$\frac{1}{80}$	0.18%	0.19%

unless the diffusive terms can balance the reaction terms. This occurs if the media have high contrast. We discuss these issues and how one can use spectral problems to define the continua. Based on obtained multicontinuum models, we show that one needs high contrast to have different average values. We derive multicontinuum models for dynamic problems with dynamic cell problems and discuss nonlinear cases. In addition, we discuss the use of both average and gradient constraints at the same time and its disadvantages. We also briefly discuss nonlinear multicontinuum models. Numerical results are presented. Our numerical results show that the proposed approach provides an accurate representation of the
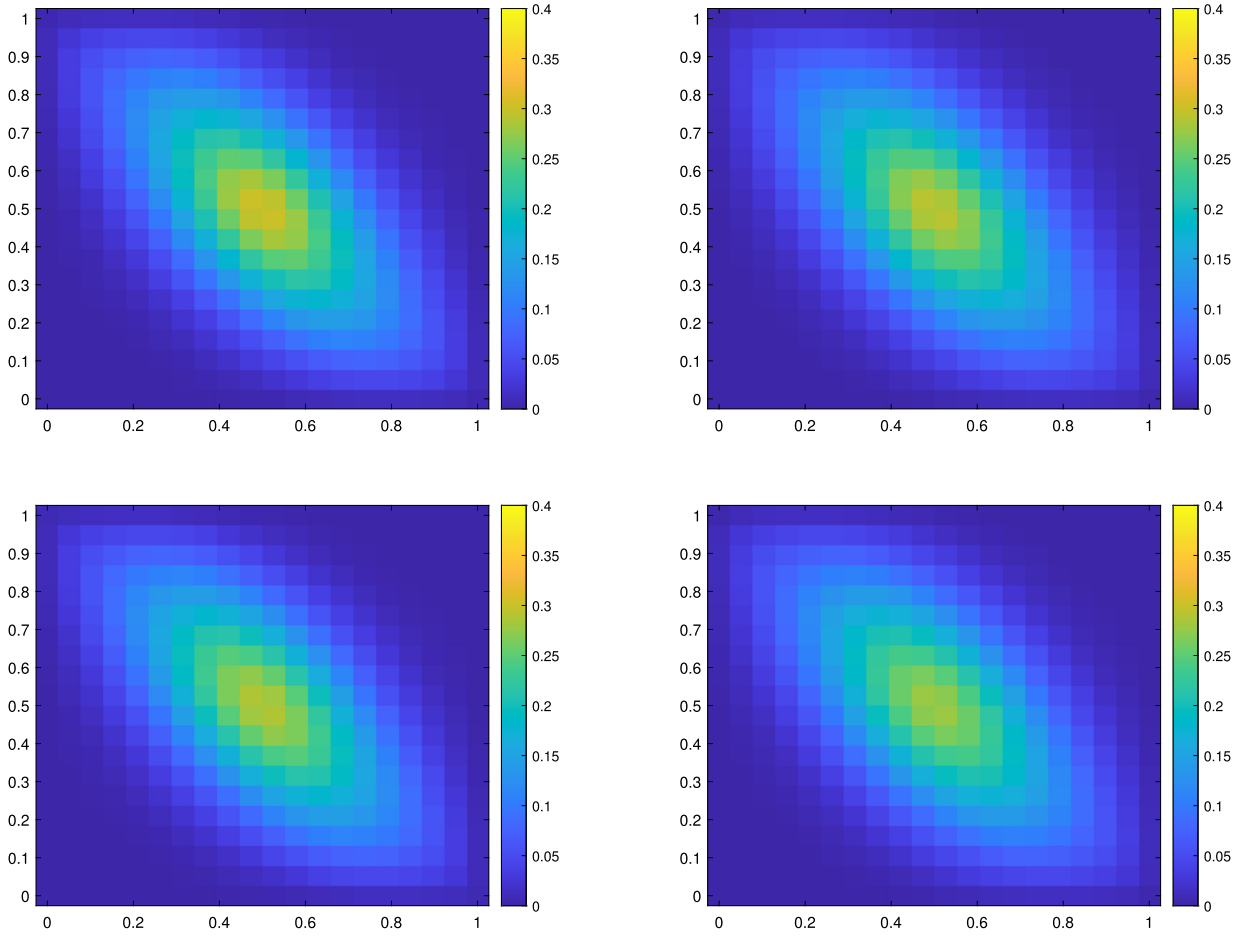
Fig. 5. Case 2. Top-Left: Reference averaged solution in Ω_1. Top-Right: Multiscale solution U_1. Bottom-Left: Reference averaged solution in Ω_2. Bottom-Right: Multiscale solution U_2.
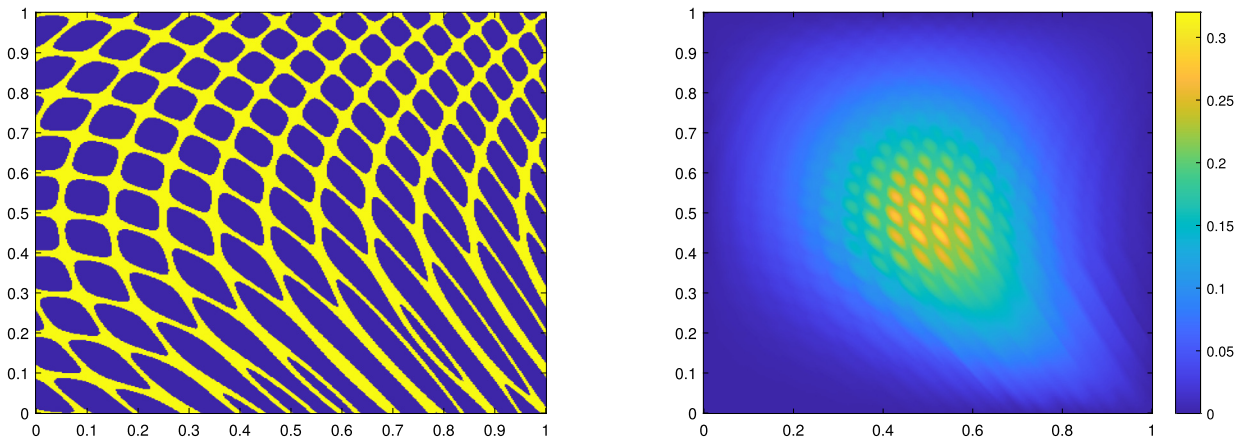
Fig. 6. Left: κ for Case 3 with $\epsilon = \frac{1}{10}$. Right: The solution snapshot.

solution's averages and converges as we decrease the mesh size. We study various parameter regimes and their influences on effective properties. Finally, we would like to note that the proposed approaches can be extended to problems without scale separation. These problems are carefully studied in our previous works [13,11].

Table 5
Effective properties α and β's. Case 2.

l	H	ϵ	$\alpha_{11}^{11}/|R_\omega|$	$\alpha_{11}^{21}/|R_\omega|$	$\alpha_{11}^{22}/|R_\omega|$
$\lceil -2\log(H)\rceil = 5$	$\frac{1}{10}$	$\frac{1}{10}$	1.4528e-04	-1.0341e-06	7.5875e-05
$\lceil -2\log(H)\rceil = 5$	$\frac{1}{10}$	$\frac{1}{20}$	1.4534e-04	-4.9526e-07	7.5874e-05
$\lceil -2\log(H)\rceil = 5$	$\frac{1}{10}$	$\frac{1}{40}$	1.4535e-04	-2.4487e-07	7.5866e-05

l	H	ϵ	$\alpha_{22}^{11}/|R_\omega|$	$\alpha_{22}^{12}/|R_\omega|$	$\alpha_{22}^{22}/|R_\omega|$
$\lceil -2\log(H)\rceil = 5$	$\frac{1}{10}$	$\frac{1}{10}$	0.0094	-0.0119	0.0192
$\lceil -2\log(H)\rceil = 5$	$\frac{1}{10}$	$\frac{1}{20}$	0.0187	-0.0239	0.0384
$\lceil -2\log(H)\rceil = 5$	$\frac{1}{10}$	$\frac{1}{40}$	0.0373	-0.0477	0.0768

l	H	ϵ	$\alpha_{12}^{11}/|R_\omega|$	$\alpha_{12}^{12}/|R_\omega|$	$\alpha_{12}^{22}/|R_\omega|$
$\lceil -2\log(H)\rceil = 5$	$\frac{1}{10}$	$\frac{1}{10}$	-1.4056e-04	2.5701e-05	-5.7296e-05
$\lceil -2\log(H)\rceil = 5$	$\frac{1}{10}$	$\frac{1}{20}$	-1.4302e-04	1.2903e-05	-6.6648e-05
$\lceil -2\log(H)\rceil = 5$	$\frac{1}{10}$	$\frac{1}{40}$	-1.4419e-04	6.4525e-06	-7.1260e-05

| l	H	ϵ	$\beta_{11}/|R_\omega|$	$\beta_{12}/|R_\omega|$	$\beta_{22}/|R_\omega|$
$\lceil -2\log(H)\rceil = 5$	$\frac{1}{10}$	$\frac{1}{10}$	0.1572	-0.1572	0.1572
$\lceil -2\log(H)\rceil = 5$	$\frac{1}{10}$	$\frac{1}{20}$	0.3145	-0.3145	0.3145
$\lceil -2\log(H)\rceil = 5$	$\frac{1}{10}$	$\frac{1}{40}$	0.6291	-0.6291	0.6291

Table 6
Error comparison for Case 3.

l	H	ϵ	$e_2^{(1)}$	$e_2^{(2)}$
$\lceil -2\log(H)\rceil = 5$	$\frac{1}{10}$	$\frac{1}{40}$	4.19%	4.24%
$\lceil -2\log(H)\rceil = 6$	$\frac{1}{20}$	$\frac{1}{40}$	1.21%	1.37%
$\lceil -2\log(H)\rceil = 8$	$\frac{1}{40}$	$\frac{1}{40}$	0.95%	1.14%

l	H	ϵ	$e_2^{(1)}$	$e_2^{(2)}$
5	$\frac{1}{10}$	$\frac{1}{10}$	5.41%	5.95%
5	$\frac{1}{10}$	$\frac{1}{20}$	4.07%	4.21%
5	$\frac{1}{10}$	$\frac{1}{40}$	4.19%	4.24%

l	H	ϵ	$e_2^{(1)}$	$e_2^{(2)}$
$\lceil -2\log(H)\rceil = 5$	$\frac{1}{10}$	$\frac{1}{10}$	5.41%	5.95%
$\lceil -2\log(H)\rceil = 6$	$\frac{1}{20}$	$\frac{1}{20}$	1.92%	2.25%
$\lceil -2\log(H)\rceil = 8$	$\frac{1}{40}$	$\frac{1}{40}$	0.95%	1.14%

CRediT authorship contribution statement

Both authors contributed to writing, editing and simulations.

Declaration of competing interest

The authors declare that they have no known competing financial interests or personal relationships that could have appeared to influence the work reported in this paper.
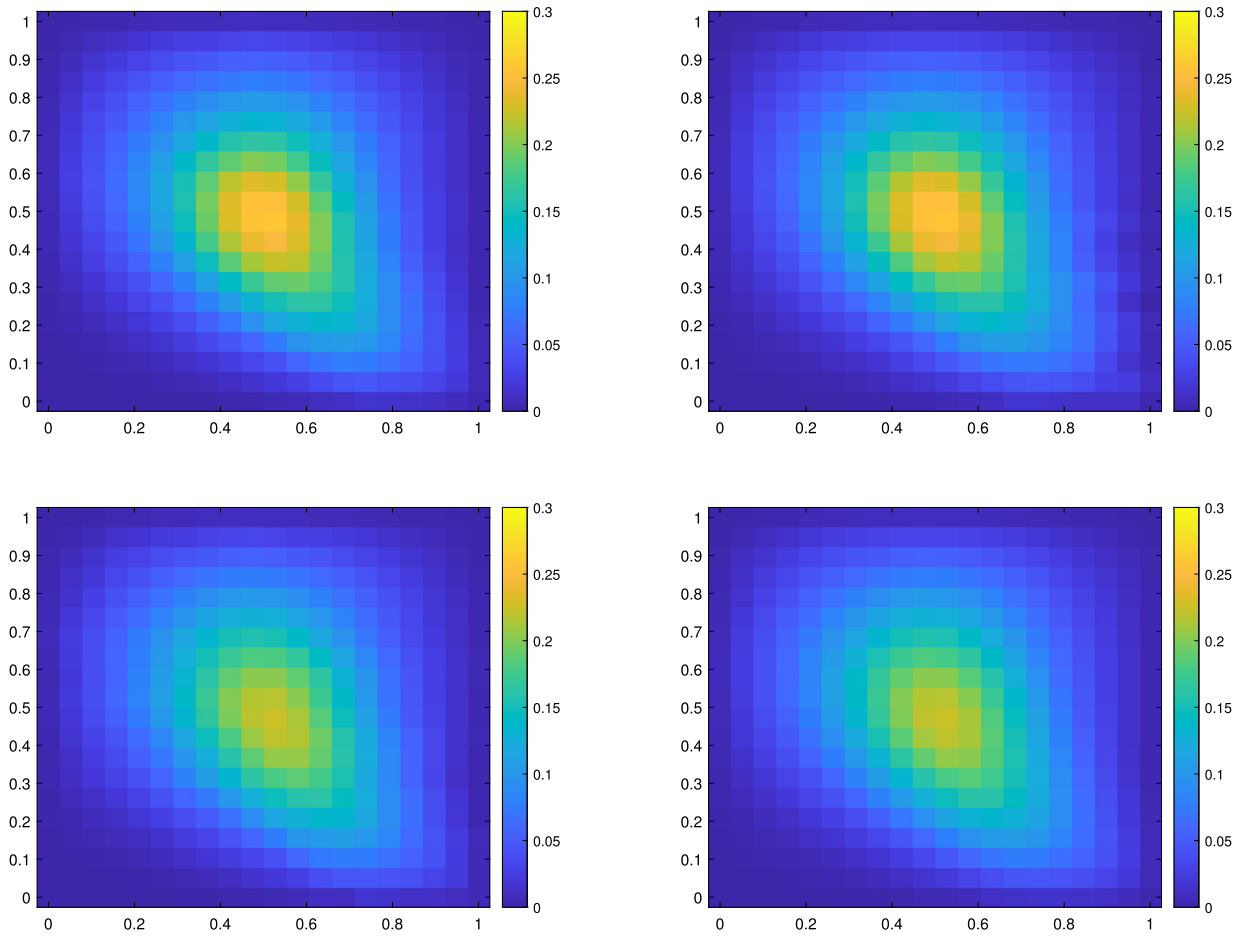
Fig. 7. Top-Left: Reference averaged solution in Ω_1. Top-Right: Multiscale solution U_1. Bottom-Left: Reference averaged solution in Ω_2. Bottom-Right: Multiscale solution U_2.

Data availability

No data was used for the research described in the article.

Acknowledgement

References

[1] E.C. Aifantis, Continuum basis for diffusion in regions with multiple diffusivity, J. Appl. Phys. 50 (3) (1979) 1334–1338.
[2] M. Alotaibi, H. Chen, S. Sun, Generalized multiscale finite element methods for the reduced model of Darcy flow in fractured porous media, J. Comput. Appl. Math. 413 (2022) 114305.
[3] T. Arbogast, J. Douglas Jr, U. Hornung, Derivation of the double porosity model of single phase flow via homogenization theory, SIAM J. Math. Anal. 21 (4) (1990) 823–836.
[4] G.I. Barenblatt, I.P. Zheltov, I. Kochina, Basic concepts in the theory of seepage of homogeneous liquids in fissured rocks [strata], J. Appl. Math. Mech. 24 (5) (1960) 1286–1303.
[5] A. Bedford, M. Stern, A multi-continuum theory for composite elastic materials, Acta Mech. 14 (2) (1972) 85–102.
[6] A. Bensoussan, J.L. Lions, G. Papanicolaou, Asymptotic Analysis for Periodic Structures, Studies in Mathematics and Its Applications, vol. 5, North-Holland, 1978.
[7] A. Bourgeat, A. Piatnitski, Approximations of effective coefficients in stochastic homogenization, Ann. Inst. Henri Poincaré Probab. Stat. 40 (2) (2004) 153–165.
[8] R. Bunoiu, C. Timofte, Upscaling of a diffusion problem with interfacial flux jump leading to a modified Barenblatt model, 2019.
[9] Z. Chai, B. Yan, J. Killough, Y. Wang, An efficient method for fractured shale reservoir history matching: the embedded discrete fracture multi-continuum approach, J. Pet. Sci. Eng. 160 (2018) 170–181.
[10] E.T. Chung, Y. Efendiev, T. Hou, Adaptive multiscale model reduction with generalized multiscale finite element methods, J. Comput. Phys. 320 (2016) 69–95.

[11] E.T. Chung, Y. Efendiev, W.T. Leung, Constraint energy minimizing generalized multiscale finite element method, Comput. Methods Appl. Mech. Eng. 339 (2018) 298–319.

[12] E.T. Chung, Y. Efendiev, W.T. Leung, M. Vasilyeva, Nonlocal multicontinua with representative volume elements. Bridging separable and non-separable scales, Comput. Methods Appl. Mech. Eng. 377 (2021) 113687.

[13] E.T. Chung, Y. Efendiev, W.T. Leung, M. Vasilyeva, Y. Wang, Non-local multi-continua upscaling for flows in heterogeneous fractured media, J. Comput. Phys. 372 (2018) 22–34.

[14] E.T. Chung, Y. Efendiev, W.T. Leung, M. Wheeler, Nonlinear nonlocal multicontinua upscaling framework and its applications, Int. J. Multiscale Comput. Eng. 16 (5) (2018).

[15] L. Durlofsky, Numerical calculation of equivalent grid block permeability tensors for heterogeneous porous media, Water Resour. Res. 27 (1991) 699–708.

[16] Y. Efendiev, J. Galvis, T. Hou, Generalized multiscale finite element methods (GMsFEM), J. Comput. Phys. 251 (2013) 116–135.

[17] Y. Efendiev, T. Hou, Multiscale Finite Element Methods: Theory and Applications, Surveys and Tutorials in the Applied Mathematical Sciences, vol. 4, Springer, New York, 2009.

[18] T. Hou, X. Wu, A multiscale finite element method for elliptic problems in composite materials and porous media, J. Comput. Phys. 134 (1997) 169–189.

[19] D. Ieşan, A theory of mixtures with different constituent temperatures, J. Therm. Stresses 20 (2) (1997) 147–167.

[20] P. Jenny, S. Lee, H. Tchelepi, Multi-scale finite volume method for elliptic problems in subsurface flow simulation, J. Comput. Phys. 187 (2003) 47–67.

[21] V. Jikov, S. Kozlov, O. Oleinik, Homogenization of Differential Operators and Integral Functionals, Springer-Verlag, 1994, Translated from Russian.

[22] W.T. Leung, E.T. Chung, Y. Efendiev, M. Vasilyeva, M. Wheeler, Space-time nonlinear upscaling framework using nonlocal multicontinuum approach, Int. J. Multiscale Comput. Eng. 17 (5) (2019).

[23] R. Lipton, Homogenization and field concentrations in heterogeneous media, SIAM J. Math. Anal. 38 (4) (2006) 1048–1059.

[24] A. Matache, C. Schwab, Homogenization via p-fem for problems with microstructure, Appl. Numer. Math. 33 (2000) 43–59.

[25] H. Owhadi, L. Zhang, Metric-based upscaling, Commun. Pure Appl. Math. 60 (2007) 675–723.

[26] G. Panasenko, Multicontinuum wave propagation in a laminated beam with contrasting stiffness and density of layers, J. Math. Sci. (2018) 1–13.

[27] L. Rubinšteın, On a question about the propagation of heat in heterogeneous media (Russian), Izv. Akad. Nauk SSSR, Ser. Geogr. Geofiz. 12 (1948) 27–45.

[28] R. Showalter, N. Walkington, Micro-structure models of diffusion in fissured media, J. Math. Anal. Appl. 155 (1) (1991) 1–20.

[29] M. Vasilyeva, W.T. Leung, E.T. Chung, Y. Efendiev, M. Wheeler, Learning macroscopic parameters in nonlinear multiscale simulations using nonlocal multicontinua upscaling techniques, J. Comput. Phys. 412 (2020) 109323.

[30] X. Wu, Y. Efendiev, T. Hou, Analysis of upscaling absolute permeability, Discrete Contin. Dyn. Syst., Ser. B 2 (2002) 158–204.

[31] L. Zhao, E.T. Chung, An analysis of the nlmc upscaling method for high contrast problems, J. Comput. Appl. Math. 367 (2020) 112480.